Radiation Physics and Chemistry 222 (2024) 111819

Contents lists available at ScienceDirect

Radiation Physics and Chemistry

journal homepage: www.elsevier.com/locate/radphyschem

An enormous increase in atmospheric positron flux during a summer thunderstorm on Mount Aragats

A. Chilingarian *, B. Sargsyan, M. Zazyan

A I Alikhanyan National Lab (Yerevan Physics Institute), Yerevan, 0036, Armenia

ARTICLE INFO

Handling Editor: Dr. Chris Chantler

Keywords:
Cosmic rays
Positrons
Accelerators

ABSTRACT

On July 11, 2023, we observed a remarkable 500% increase in positron flux, coinciding with a significant Thunderstorm Ground Enhancement (TGE). The enhanced flux of electrons and gamma rays was attributed to relativistic runaway electron avalanches (RREAs) generated within the dipole formed between the main negatively charged layer in the middle of the thundercloud and the Lower Positively Charged Region (LPCR) at the bottom of the thundercloud. Concurrently, a substantial enhancement in the 511 keV gamma-ray flux resulting from electron-positron annihilation was recorded. This surge is intricately linked to the LPCR within the thundercloud. The emergence of the LPCR induces a polarity change in the atmospheric electric field (AEF) below the LPCR (fourth dipole), leading to the deceleration of electrons and the acceleration of positrons.

Particle flux measurements were conducted using scintillation and NaI(TL) spectrometers. To mitigate the contamination of natural gamma radiation and refine the 511 keV flux measurements, the ORTEC spectrometer was shielded with a 4 cm thick lead filter. CORSIKA simulations corroborate the observed positron flux enhancement.

Highlighting the synergy between high-energy physics in the atmosphere and astroparticle physics, we introduce a new scenario to elucidate the enigmatic large flux of galactic positrons measured by the Alpha Magnetic Spectrometer (AMS) aboard the International Space Station (ISS).

1. Plain Language summary

Cosmic rays encountering atmospheric electric fields can undergo substantial increases, sometimes by orders of magnitude within minutes and by significant percentages over hours. Tracking the charge evolution within thunderstorms poses challenges due to their rapid and dynamic nature, compounded by the difficulty of direct measurements. Leveraging cosmic rays as universal indicators, we monitored changes in atmospheric charge structure during thunderstorms.

Our investigation revealed a remarkable surge in positron flux coinciding with the emergence of a mature Lower Positively Charged Region (LPCR) within thunderstorms. Particularly noteworthy was the observation that the dipole formed between the LPCR and the Earth's surface led to a profound enhancement in positron flux, marking the first documented instance of such a phenomenon.

This research advances our fundamental understanding of atmospheric physics and bears practical implications. It enhances our ability to predict and mitigate the impacts of severe weather phenomena and sheds light on analogical phenomena in high-energy astroparticle physics.

2. Key points

- We identify a fourth dipole in the lowest part of the atmospheric electric field (AEF).
- The fourth dipole between the lower positively charged region and the ground decelerates electrons.
- A 500% surge in positron flux during thunderstorms was observed within the fourth dipole on July 11, 2023.
- When the AEF decelerates electrons, bremsstrahlung, and pair production intensify significantly.
- CORSIKA simulations corroborate the substantial boost in positron flux within the fourth dipole.
- We propose a novel scenario to explain the large flux of galactic positrons measured by the Alpha Magnetic Spectrometer (AMS).

* Corresponding author.
E-mail address: chili@aragats.am (A. Chilingarian).

https://doi.org/10.1016/j.radphyschem.2024.111819
Received 24 January 2024; Received in revised form 2 April 2024; Accepted 30 April 2024
Available online 7 May 2024

3. Introduction

At the beginning of the last century, C.T.R. Wilson discovered that an atmospheric electric field (AEF) applied in the direction of electron motion would add to the atmospheric electron energy sufficient to counterbalance ionization losses (Wilson, 1925). Wilson proposed that the Earth acts as a source of negative charge due to the beta radiation of the radon progeny emanating from the ground and the deposition of negative ions by precipitation. This negative charge forms a layer near the Earth's surface. Above the negative surface layer, Wilson suggested the existence of a layer of positive charge, which he attributed to processes such as ionization by cosmic rays and the transport of positive ions aloft by convection. The AEF between these "Wilsonian layers" (Wilson, 1921) accelerates free electrons upward toward the open space. Thus, the flux of electrons and positrons is modulated by electrostatic fields arising in the atmosphere, which are governed by the charge structures within thunderclouds. In the early stages of particle interaction theory development, when the radiation losses and particle avalanches in the atmosphere were poorly understood, the Wilsonian model of electron acceleration suffered from overestimating the expected gain in electron energy. This led to negative results in observing electron flux on the Earth's surface due to inadequate experimental arrangements. The experiments in South Africa (Schonland, 1930; Schonland and Viljoen, 1933; Halliday, 1934, 1941) fail to measure relativistic electron flux during thunderstorms. Only after 100 years was the energy spectrum of boosted atmospheric electrons measured on Aragats (Chilingarian et al., 2010, 2011).

AEF investigations atop Germany's highest peak, Zugspitze (1945–1948), challenged the prevailing understanding of cloud charge distribution. Joachim Küttener's experiments unveiled a more complicated intracloud electric field, deviating from the conventional Wilsonian layers (Küttener, 1950). He identified a transient Lower Positive Charge Region (LPCR) in the bottom of the cloud, formed by a positive charge on graupel, a specific state of water characterized by an ice shell. Subsequent studies (Nag and Rakov, 2009) affirmed the tripole structure of cloud charge, highlighting the role of "graupel" hydrometeors in LPCR formation. The discovery of the LPCR and subsequent refinement of the tripole model marked a significant paradigm shift in atmospheric science. With its Main Negatively Charged Layer (MN), LPCR, and Main Positively Charged Layer (MP), the tripole model elucidates the particle modulation and lightning initiation. The MN-MP dipole propels electrons toward open space (first dipole), while the MN-LPCR and MN-MIRR dipoles accelerate electrons earthwards (second and third dipole). All three dipoles create relativistic runaway electron avalanches (RREAs, Gurevich et al., 1992; Babich et al., 2001; Alexeenko et al., 2002; Dwyer, 2007). RREAs cause a sizeable impulsive enhancement of the electrons and gamma rays registered on Earth's surface by particle detectors and spectrometers as thunderstorm ground enhancements (TGEs, Chilingarian et al., 2010, 2011). TGEs developing in the large-scale AEF consist of billions of gamma rays, electrons, positrons, and rarely neutrons. RREA started when electric field strength exceeded a critical value specific to the air density (Roussel-Dupré et al., 1998; Dwyer, 2003; Babich et al., 2004). Balloon experiments conducted in New Mexico (Marshall et al., 1995; Stolzenburg et al., 2007) and TGEs detected on Aragats (Chilingarian et al., 2019a, 2022a, 2023a), Zugspitze (Chilingarian et al., 2024), Musala (Chilingarian et al., 2021a) and Lomnicky Stit mountains (Chum et al., 2020) demonstrate coherence of strong AEFs and emerging particle fluxes. Numerous simulations have also demonstrated the exponential increase in particle numbers after the modeled electric field surpasses the critical value through distances of 1–2 km (Chilingarian et al., 2021b, 2021c).

In the present research, we investigate the modulation of particles by a fourth dipole between LPCR and its mirror on the Earth. The evolution of LPCR is discernible in the transition from negative to positive near-surface electric field (NSEF) readings captured by BOLTEK's EFM-100 sensor (BOLTEK, 2024). This sensor, widely employed in atmospheric physics research, measures NSEF and distance to the lightning flash up to 33 km with a 20 Hz frequency. NSEF data, transmitted via WiFi, is stored in a MySQL database. Typically, 1-s averaged NSEF time series are used for multivariate visualization and correlation analysis. Weather parameters are recorded by the DAVIS weather station (DAVIS, 2024) and stored as a 1-min time series for the correlation analyses and spread (difference between outside temperature and dew point) calculation.

For natural gamma-ray radiation (NGR) spectroscopy, the ORTEC-905-4 spectrometer is employed. This gamma spectrometer features a $3'' \times 3''$ NaI (Tl) crystal, 1024 measuring channels, and a relative energy resolution of FWHM (full width at half maximum) 7–10% at energy levels of 0.3–1.5 MeV (Hossain et al., 2012). To suppress contamination of 511 keV gamma rays from Compton scattered gamma rays from the Radon decay chain, a 4 cm thick lead brick enclosure surrounds the spectrometer from the bottom and all sides, leaving only the top open.

The TGE particle fluxes were measured with a STAND1 network of stacked 1 m^2 area and 1 cm thickness scintillators covering a 50 000 m^2 area at the Aragats research station (Chilingarian et al., 2022c). Energy spectra of TGE gamma rays and electrons are measured with two 0.25 m^2 area and 20 cm thickness scintillators equipped with 1 m^2 area and 1 cm thickness "veto" scintillator (Chilingarian et al., 2024a). A logarithmic amplitude-to-digit converter (LADC) is a key component of spectrometer electronics, allowing energy release measurements from 0.3 to 50 MeV.

4. Extreme TGE on July 11, 2023

After detecting the ≈20% enhancement of the positron flux during the minor TGEs in June 2023 (Chilingarian and Sargsyan, 2024b), a substantial TGE event, significantly surpassing the fair-weather flux, was documented on July 11, 2023. Fig. 1 illustrates the dynamics of the NSEF disturbances (black curve) and corresponding particle flux enhancement (blue curve). NSEF started to rise at 4:46, and at 4:47–4:49 was in the positive domain (shown by vertical green lines). The corresponding surge in the count rate was delayed by approximately 40 s and correlated well with the NSEF rise. At the peak enhancement, TGE particle flux surpasses the fair-weather flux ≈2.3 times, escalating from 550 to 1250 counts per second. During the TGE's decaying phase at 4:49:10, the NSEF was in the negative domain (outlined by yellow lines in Fig. 1). Notably, the count rate gradually decays, exhibiting a slower decline than the NSEF.

At the positive NSEF, the positive charge accumulates above the detectors, intensifying the electric field strength in the lower dipole MN-LPCR. Concurrently, the dipole between LPCR and its Earth mirror decelerates electrons and accelerates positrons. At the negative NSEF, the MN-MIRR dipole continues to accelerate electrons within the cloud until smoothly decaying at 4:51. This large TGE, encompassing both positive and negative NSEF periods, provides an opportunity to compare the operation of the different electron-positron accelerators at distinct charge structures within the thundercloud.

Usually, we gauged TGE intensity through a 1-s time series of count rates (Fig. 1). In this study, we adopt a more granular approach, utilizing a 50 ms time series to follow the details of the count rate dynamics throughout several tens of seconds. Fig. 1 showcases the overall behavior of the TGE particle flux, while Fig. 2 provides its detailed narrative with the 50-ms time series capturing the stability of the TGE development (upper time series). These representations are compared with the count rate during fair weather, measured simultaneously on the preceding day (lower time series). For our analysis, we have identified a 42-s interval during the peak flux of TGE, wherein the electron accelerator maintained a consistent flux. In this brief window, the flux experienced a remarkable enhancement of 130%, exhibiting a significance of 5.45σ. Extrapolating this stable flux to a minute (for comparative purposes) would elevate the significance of the 1-min peak to an impressive 189σ. A noteworthy aspect of the TGE flux lies in its relative standard deviation (RSD), which stands at 16%, in contrast to the 24%

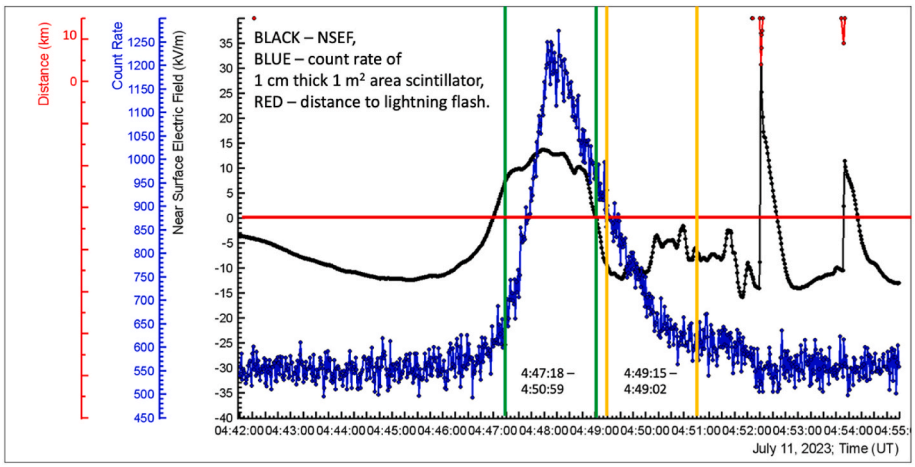

Fig. 1. One-second time series of STAND1's upper scintillator's count rate (blue) and NSEF (black). Vertical green and yellow lines indicate times of positive and negative NSEF, and the horizontal red line separates the positive and negative domains of NSEF.

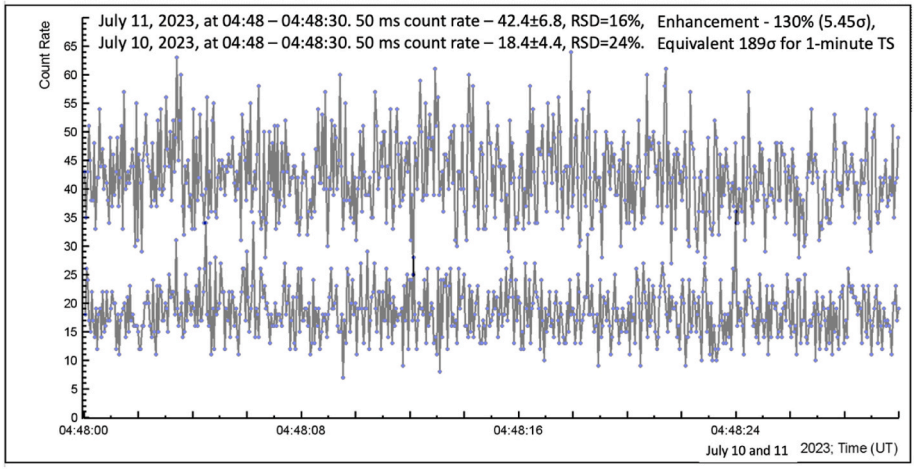

Fig. 2. 50 ms time series of count rates of STAND1's upper scintillator at TGE and fine weather. The legend shows the count rate's mean value, standard deviation, and relative standard deviation.

observed during fair weather. This implies that the flux from the atmospheric electron accelerator during 42-s interval exhibits greater stability than the ambient population of cosmic rays.

5. Localization of the electric field in thundercloud

In the dynamic environment of thunderstorms, the complex process of charge separation and accumulation leads to the amplification of electric fields in the lower atmosphere. Precisely localizing these electric fields within a cloud is pivotal for the comprehensive study of AEF and RREA, accurate prediction of weather patterns, and effective assessment of risks associated with severe weather phenomena triggered by thunderstorms.

Due to thunderstorms' stochastic nature, achieving sub-kilometer accuracy has historically been a significant feat. In this section, we introduce innovative techniques designed to precisely localize the lower boundary of the strong electric field within a thundercloud. Registering TGEs from the electron accelerator within the cloud, we employ recovered electron and gamma-ray energy spectra to estimate the height of the strong electric field above the ground with an impressive accuracy of ≈50 m (Chilingarian et al., 2021c).

To determine the Free Path Distance (FPD), at which the accelerating field terminates and RREA traverses dense air until it reaches the ground, we employ an empirical equation (1) whose parameters were also fitted by simulations.

$$\mathrm{FPD\ (meters)} = (C_1 * E^{\gamma}_{max} - E^{e}_{max})/C_2 \quad (1)$$

The coefficients C_1 and C_2 are empirically estimated as 1.2 and 0.2 MeV/m, respectively. Notably, our TGE simulations indicate that the maximum energy of electrons exiting the electric field surpasses that of gamma rays by 20%. Consequently, we estimate the maximum energy of electrons leaving the field by $C_1 * E^{\gamma}_{max}$.

Additionally, we make key assumptions: first, that gamma rays' maximum energy remains relatively constant when traveling 100 m or less in the atmosphere, and second, that electrons experience an approximate energy loss of 0.2 MeV per meter at altitudes around 3000–3500 m.

Fig. 3 represents the recovered gamma ray and electron spectra and corresponding maximum energies at the minute of the maximum flux achieved at positive and negative NSEFs. The FPD at positive and negative NSEF, according to the corresponding maximum energies and equation (1), are 90 and 55 m, consequently. More intriguing is the percentage of electrons relative to gamma rays. For positive NSEF it equals 1774/152290 ≈ 1.2%; for negative NSEF – 982/23700 ≈ 4.2%. Thus, electron flux decelerated and diminished in the gap between LPCR and the ground.

The cloud base height is determined by calculating the difference

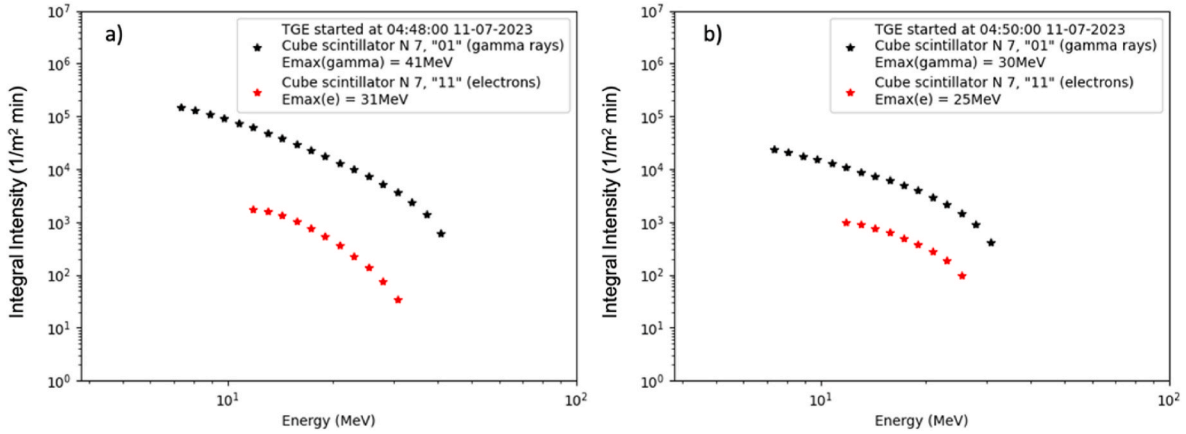

Fig. 3. a) integral energy spectra of electrons and gamma rays at positive NSEF and negative NSEF b). The total number of electrons and gamma rays are (1774, 152290) at NSEF+ and (982, 23700) at NSEF$^-$.

between air temperature and dew point. This approach is grounded in a well-known approximate equation (2) (Spread, 2024), where the cloud base height H is estimated as:

$$H(m) \approx (\text{Air temperature at surface } \{\circ C\} - \text{dew point temperature } \{\circ C\}) \times 122 \quad (2)$$

The computed difference (spread) between air temperature and dew point indicates the cooling required for condensation. It's important to note that this method assumes a linear and uniform decrease in temperature with altitude, which might not perfectly represent the complexity of real atmospheric conditions featuring local variations.

In Fig. 4, we present the 1-min time series of weather parameters. Two symmetric black curves represent the outside temperature and dew point. During the TGE event, solar radiation was negligible (green curve), indicating substantial cloud coverage. Relative humidity stood at 97% (blue curve), and the outside temperature was recorded at +4.2 °C. No rainfall or lightning flash was detected during this period. In the inset, we show a cloud base height time series. The red arrows show the TGE time.

By applying Equation (2), we estimate the cloud base height to be approximately 70 m. The consistency in estimates of the FPD and cloud base height suggests a gradual weakening of the intracloud electric field as it approaches the Earth's surface. Large TGE flux, observed during positive NSEF, provides evidence of the emergence of the mature LPCR and the formation of a fourth dipole between LPCR and its mirror in the Earth.

This dipole accelerates positrons toward the Earth and decelerates electrons. To gauge positron flux intensity, we rely on the flux of its proxy—the "annihilation" 511 keV gamma rays, which are measured by the ORTEC precise spectrometer.

6. Measurement of the natural gamma radiation and the annihilation 511 keV line

In Fig. 5, we present 1-s spectrograms of NGR at positive and negative NSEF, measured by the ORTEC spectrometer over 105 s. We

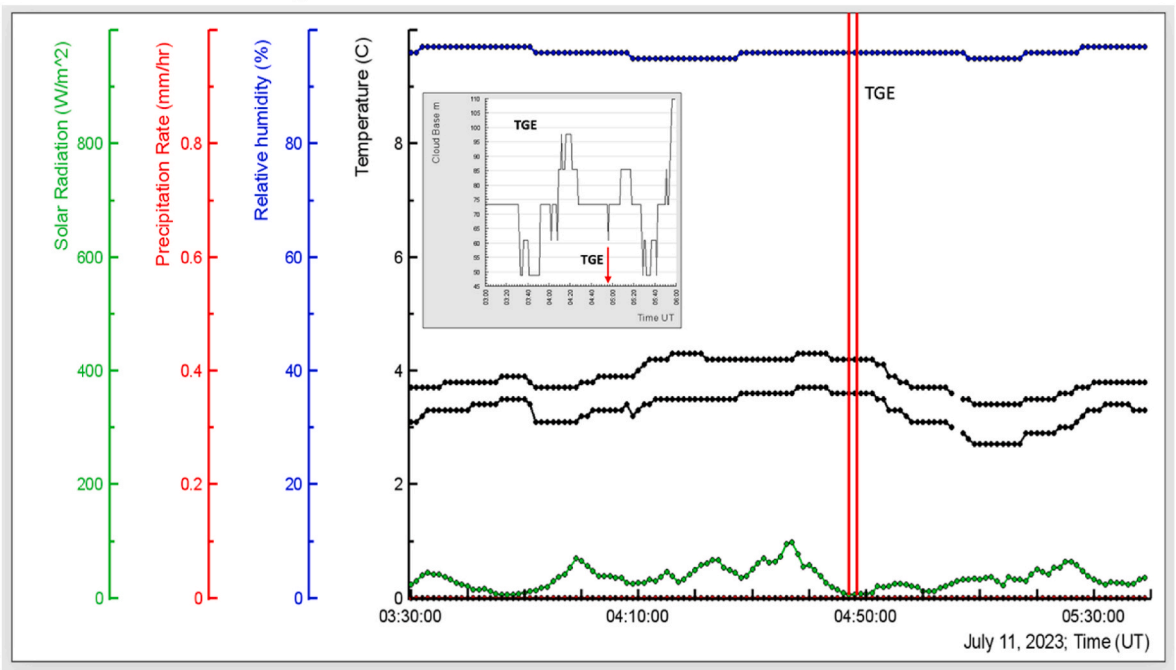

Fig. 4. A 1-min time series of outside temperature and dew point (black curves), relative humidity (blue curve), rain rate (red curve), and solar radiance (green curve). In the inset, we show the changing height of the cloud base calculated by equation (2). Red vertical lines and red arrows indicate the TGE time.

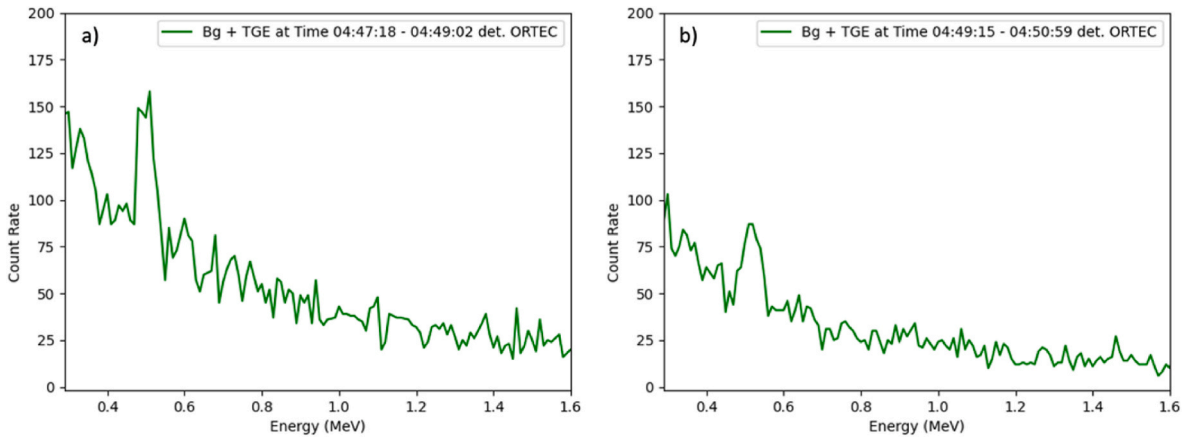

Fig. 5. NGR spectrograms obtained with the ORTEC spectrometer during positive a) and negative b) NSEF, as indicated by lines in Fig. 1 (each period equals 105 s). The histogram bin width equals 10 keV.

segregate the spectrograms for times of positive NSEF (Fig. 5a) and negative NSEF (Fig. 5b).

The 511 keV annihilation line is notably more pronounced at positive NSEF than negative NSEF, further supporting the correlation between LPCR emergence and enhanced positron intensity. The 511 keV lines are well pronounced due to suppression of the gamma radiation from Radon progeny, which is absorbed by the lead filter enveloping the ORTEC spectrometer. This "background-free" spectrographic analysis provides valuable insights into the dynamics of charge structures within the thundercloud during TGE events.

Table 1 compares radionuclide and 511 keV line enhancements during positive (TGE1) and negative (TGE2) NSEF measured for 105 s each. The second row shows the energy range for selecting isotopes and the 511 keV gamma rays. In the next row, we show the intensity of the gamma rays measured at fair weather after TGE (04:05:00–04:06:45) and at positive and negative NSEF. The two last rows show the intensity enhancement relative to fair weather. The 511 keV gamma rays reveal a remarkable 500% enhancement during positive NSEF and a 150% enhancement during negative NSEF, underscoring the substantial influence of emerging LPCR and fourth dipole on the positron flux bust. We also confirm our finding (Chilingarian and Sargsyan, 2024b) that negative aerosols more effectively lift radon progeny to the atmosphere than positive ones. The NSEF lifts aerosols into the atmosphere, and precipitation returns them (radon circulation effect, Chilingarian et al., 2020).

7. Simulation of the influence of the fourth dipole on TGE Particle flux

Monitoring RREA development within thunderclouds is challenging. Therefore, combining simulations of RREA development in the thundercloud with measured TGE particle intensities on Earth's surface offers valuable insights into AEF strength and extension (Chilingarian et al., 2021c; see Figs. 2 and 3). Using CORSIKA simulations (Heck et al., 1998), we explore possible RREA scenarios above Aragats, introducing a uniform electric field at 5300 m above particle detectors at 3200 m. We vary the strengths and extensions of the intracloud electric field and consider FPD for RREA electrons and gamma rays in dense air before reaching the ground from 50 to 200 m.

Based on the RREA threshold electric field of 284 kV/m at sea level and an air density of 1.225 kg/m^3, we calculate a critical field of 1.70 kV/cm at 5300 m (air density 0.7364 kg/m^3). The modeled AEF of 2.20 kV/cm exceeds the critical value by approximately 30%. At 3200 m (air density 0.9093 kg/m^3), the critical electric field strength is 2.10 kV/cm, exceeding the threshold by approximately 5%.

For an introduced uniform electric field of 1.90 kV/cm at 5300 m, the energy is only 6% higher than the critical value; at 4000 m, it matches the critical energy. Consequently, electron acceleration ceases, with maximum electron and gamma-ray energies not exceeding 30 MeV. For higher electric field strengths, RREA electrons can reach energies of approximately 70 MeV and gamma-rays around 50 MeV, resulting in electrons having about a 20% higher maximum energy than gamma rays upon exiting the accelerating field. Subsequently, in dense air, electron energies diminish rapidly due to ionization losses, whereas gamma-ray energies remain relatively stable for FPDs up to 100 m.

In our previous work (Chilingarian et al., 2021b, Fig. 5 and Table 2), we directly compared simulations with experimentally measured spectra. For lower electric field strengths (1.8 and 1.9 kV/cm), the RREA process attenuates before reaching the observation level at 3200 m (refer to green and brown curves in Fig. 5a of Chilingarian et al., 2021b). Thus, for smaller TGE events (observed in the summer of 2020), the accelerating electric field extends less than 1500 m, with a potential drop in the cloud of less than 250 MV.

We estimated the maximum atmospheric electric field strength in our study at Mt. Lomnicky Stit in Slovakia (2600 m). Comparing simulations with a large TGE event registered by the SEVAN detector (Chum et al., 2020; Chilingarian et al., 2018), we determined a potential drop of 500 MV (see Figs. 5 and 6, Table 2 of Chilingarian et al., 2021a).

Table 1
Enhancements of radionuclides and 511 keV line measured on July 11, 2023 during 10 s of positive and negative NSEF.

ORTEC Count Rate 105sec	0.511 k MeV	214 Pb 0.352 MeV	214Bi 0.609 MeV	sum of radionuclides 0.7–3 MeV	CR + Compton scatter	SUM 0.3–3 MeV
Energy range (MeV)	[0.47–0.55]	[0.32–0.38]	[0.56–0.66]	[0.7–3]	[0.3–3]	[0.3–3]
Bg at time 04:05:00–04:06:45	80	49	46	99	2084	2358
Bg + TGE1 at time 04:47:18–04:49:02	475	172	115	304	8389	9455
Bg + TGE2 at time 04:49:15–04:50:59	281	81	65	195	4563	5185
Enhancement TGE1 (%)	500	250	150	207	213	266
Enhancement TGE2 (%)	150	65	41	96	119	120

Table 2
The number of particles reaching the observation level at 3200 m per initial 1 MeV seed electron.

Run number	Ez (kV/cm) at different heights	Number e + per seed	Number e-per seed	e+&e- per seed	Number γ per seed
1	+2.1 kV/cm (3300–5300m)	0.07	1.94	2.00	142.4
2	+2.1 kV/cm (3300–5300m) −2.0 kV/cm (3200–3300m)	0.35	0.57	0.92	124.1
3	+2.2 kV/cm (3300–5300m)	0.8	28.8	29.7	1452.8
4	+2.2 kV/cm (3300–5300m) −2.0 kV/cm (3200–3300m)	3.9	6.6	10.5	1355.11
2/1		5	0.3	0.46	0.87
4/3		4.9	0.23	0.35	0.93

Thus, through extensive RREA simulations and comparisons with recovered TGE energy spectra, we identify characteristics of TGE (maximum energies) associated with AEF strength and location. These comparisons confirm an overall intracloud electric field strength of 1.8–2.2 kV/cm and an extension of 1–2 km for TGEs observed on Aragats.

In this study, we simulated particle propagation through the two dipoles to estimate the influence of the fourth dipole on TGE particle flux. The first dipole is between the main negatively charged layer in the middle of the thundercloud and the lower positively charged layer. This dipole accelerates electrons downward toward the Earth's surface. Upon leaving this electron-accelerating field, TGE particles enter an electric field of the opposite direction, accelerating positrons and decelerating electrons.

To ensure accuracy, we conducted the simulation in two independent versions. In the first version, we used electrons with an energy of 1 MeV entering an electric field of 2.1 and 2.2 keV/cm at an altitude of 5300 m. The second version simulates the interactions of primary protons with an energy of 1000 TeV in the terrestrial atmosphere. The particles from the resulting extensive air showers (EASs) enter the same electric field. For comparison purposes, we also conducted both simulations in a "pure" mode, considering only the electron-accelerating field. The energy cutoff of secondary particles is the same for both simulations: 0.3 GeV (hadrons), 0.01 GeV (muons), and 50 KeV (electrons, positrons, and gamma rays). The Zenith angle was: $\theta = 0^{\circ}$. Number of simulation trials for seed electrons was 10 000. Tables 2 and 3 present the results of these simulations. We consider electron propagation in a 2.0 kV/cm decelerating field after acceleration in the extended acceleration field of 2.1 kV/cm and 2.2 kV/cm.

Table 3
Number of particles reaching observation level at 3200 m, from EAS initiated by a primary proton with energy, Eo = 10^5 GeV.

Run number	Ez (kV/cm) at different heights	Number e+	Number e−	Number e+&e−	Number γ
100	0	0.1 10^5	0.2 10^5	0.3 10^5	2.76 10^5
101	+2.1 kV/cm (3300–5300m)	0.21 10^5	2.65 10^5	2.86 10^5	156.2 10^5
102	+2.1 kV/cm (3300–5300m) −2.0 kV/cm (3200–3300m)	0.6 10^5	0.9 10^5	1.5 10^5	144.5 10^5
103	+2.2 kV/cm (3300–5300m)	0.24 10^5	6.8 10^5	7.0 10^5	329.8 10^5
104	+2.2 kV/cm (3300–5300m) −2.0 kV/cm (3200–3300m)	1.2 10^5	1.9 10^5	3.110^5	356.2 10^5
102/101		3.5	0.34	0.53	0.93
104/103		5.0	0.28	0.44	1.08

Both simulations show good agreement. In the last 2 rows, we show the ratio of the observed particles in the composite electric field (including the inverse field in the lowest dipole) to the "pure" dipole. A notable observation is the significant enhancement of positron flux and suppression of electron flux, with little change observed in bremsstrahlung gamma-ray flux. The positron flux enhancement obtained in both simulation versions agrees with the measured one on July 11, 2023.

The process of bremsstrahlung radiation is essentially the same whether the electric field is positive or negative; however, the effects on the particle's motion and the resulting radiation can differ. In a positive electric field (accelerating field), electrons will be accelerated in the direction of the field and gain kinetic energy. When these electrons decelerate due to interactions with atomic nuclei or other particles, they emit bremsstrahlung radiation. The energy of the emitted radiation will be proportional to the energy lost by the decelerating electron.

In a negative electric field (decelerating field), electrons moving through the field will experience a force opposing their motion, causing them to slow down. As these electrons decelerate, they emit bremsstrahlung radiation as well. The difference here is that electrons in a negative electric field are already losing kinetic energy due to the field's opposing force, leading to increased deceleration and, thus, potentially more intense bremsstrahlung radiation than a positive electric field of similar strength.

When a high-energy photon interacts with an atomic nucleus in a negative electric field, pair production can also be influenced. The decelerating field may affect the trajectories and energies of the produced electron and positron, potentially leading to different energy distributions compared to pair production in an accelerating field.

Consequently, the increased flux of gamma rays significantly contributes to producing electron-positron pairs, explaining the huge positron flux measured during the July 11, 2023 TGE event.

8. Discussion and conclusions

Understanding and predicting severe weather events, including lightning initiation and associated hazards, crucially depends on the meticulous study of electric field strength and localization within thunderclouds. Previous investigations have revealed the modulatory role of the AEF on various cosmic ray phenomena, encompassing cosmic ray electrons and gamma rays (Chilingarian et al., 2012a), natural gamma-ray radiation (Chilingarian and Sargsyan, 2024c), atmospheric muons (Chilingarian et al., 2021d) and neutrons (Chilingarian et al., 2012b).

Our research has identified a significant correlation between the emergence of an LPCR—originally discovered by Joachim Küttner in the lower part of thunderclouds and the modulation of positron flux. Utilizing energy spectra measurements of electrons and gamma rays, we could estimate the boundary of a robust accelerating electric field of 2.1–2.2 kV/cm positioned 50–90 m above the ground, coinciding with the cloud base at 50–100 m.

The enhanced flux of 511 keV gamma rays strongly suggests the origination of a fourth dipole between the LPCR and the ground. Thunderstorm-generated electrons, accelerated and multiplied within dipoles located within the thundercloud, enter the oppositely directed fourth dipole. Here, they undergo intense bremsstrahlung and pair production processes. This leads to significant attenuation of the electron flux and enhancement of the positron flux.

Our observations reveal that when LPCR and the fourth dipole emerge, the positron flux, estimated via 511 keV annihilation gamma rays, exhibits a 500% enhancement during positive NSEF. Conversely, during negative NSEF, only a 150% enhancement is recorded.

Furthermore, our research highlights the differential efficiency of pair production in the electron accelerated and decelerated fields. Electrons in a decelerated field emit bremsstrahlung radiation more efficiently. Some of the emitted gamma rays possess sufficient energy to undergo pair production near atomic nuclei, resulting in a higher production rate of electron-positron pairs compared to when no decelerating field is present.

Consequently, our spectrometric measurements of cosmic rays traversing the AEF offer precise insights into the field's strength and localization, demonstrating the emergence of the fourth dipole between LPCR and the Earth's surface. These findings contribute significantly to our understanding of atmospheric electricity and its impact on particle interactions within thunderclouds.

Our previous publication (Chilingarian, 2023) emphasized the importance of synergy between high-energy physics in the atmosphere and high-energy astrophysics. The measured bust of positron flux gives another example of this synergy. One of the intriguing observations made by the Alpha Magnetic Spectrometer (AMS) aboard the International Space Station (ISS) is the measurement of an unexpectedly high flux of positrons (Aguilar et al., 2019). Several hypotheses have been proposed to explain this unexpected result.

- Dark Matter Annihilation: some theories suggest that dark matter particles may annihilate or decay into standard model particles, including positrons and electrons.
- Astrophysical Sources: Pulsars, black hole jets, and supernova remnants (SNRs) are known to produce high-energy particles, including positrons. Their enhanced activity or unusual properties could contribute to the observed high positron flux.
- Secondary Production in Cosmic Ray Interactions: Cosmic rays can interact with interstellar gas and produce secondary particles, including positrons. Variations in cosmic ray flux or interactions with specific regions of the interstellar medium could influence the observed positron flux.

Our results suggest an additional scenario for the elevated positron flux: the deceleration of electron flux in the electric fields emerging in space plasmas. Strong electric fields can emerge in most potential sources of relativistic electrons, producing abundant positrons.

- Particles accelerate within supernova remnants (SNRs) at the shock front produced by the interaction between the supernova ejecta and the interstellar medium. However, emerging electric fields can potentially decelerate electrons in certain regions where the shock is decelerating or encountering obstacles.
- Strong magnetic fields near neutron stars can induce localized electric fields, in which electrons can experience acceleration or deceleration.
- Black hole jets are characterized by intense magnetic fields and localized electric fields. In these regions, electrons can experience deceleration or acceleration depending on the interplay between electric and magnetic fields and the surrounding environment.

Charges can be separated in areas with varying magnetic fields in all three cosmic ray sources. This separation leads to the emergence of electric fields, which can influence the motion of electrons. The field's direction and strength can cause the electrons to accelerate or decelerate. Although the AMS results refer to much higher energies, electric fields in exotic galactic sources are expected to be much stronger than those in the terrestrial atmosphere.

CRediT authorship contribution statement

A. Chilingarian: Writing – review & editing, Writing – original draft, Visualization, Supervision, Project administration, Investigation, Formal analysis, Conceptualization. **B. Sargsyan:** Visualization, Validation, Software, Investigation, Formal analysis. **M. Zazyan:** Investigation, Formal analysis, Software.

Declaration of competing interest

The authors declare that they have no known competing financial interests or personal relationships that could have appeared to influence the work reported in this paper

Data availability

Data will be made available on request.

Acknowledgments

We want to express our gratitude to the Aragats Space Environmental Center staff. Their dedication has ensured the smooth operation of our experimental facilities on Mount Aragats. The data used in this study can be accessed through the ADEI multivariate visualization software platform hosted on the Cosmic Ray Division (CRD) webpage. Interested readers are encouraged to explore the dataset (ADEI, 2024).

The Higher Education and Science Committee of Armenia, through Research Project No. 21AG-1C012, supports this research project.

References

ADEI. Available online: http://adei.crd.yerphi.am/. (Accessed 1 January 2024).

Aguilar, M., Ali, Cavasonza L., Ambrosi, G., et al., 2019. Towards understanding the Origin of cosmic-ray positrons. Phys. Rev. Lett. 122, 041102 https://doi.org/10.1103/PhysRevLett.122.041102.

Alexeenko, V.V., Khaerdinov, N.S., Lidvansky, A.S., et al., 2002. Transient variations of secondary cosmic rays due to atmospheric electric field and evidence for pre-lightning particle acceleration. Phys. Lett. 301, 299–306. https://doi.org/10.1016/S0375-9601(02)00981-7.

Babich, L.P., Donskoy, E.N., Kutsyk, I.M., et al., 2001. Comparison of relativistic runaway electron avalanche rates obtained from Monte Carlo simulations and kinetic equation solution. IEEE Trans. Plasma Sci. 29 (3), 430. https://doi.org/10.1109/27.928940.

Babich, L.P., Donskoy, E.N., Il'kaev, R.I., Kutsyk, I.M., Roussel-Dupré, R.A., 2004. Fundamental parameters of a relativistic runaway electron avalanche in air. Plasma Phys. Rep. 30, 616–624. https://doi.org/10.1134/1.1778437.

BOLTEK, available online: https://www.boltek.com/EFM-100C_Manual_030323.pdf (accessed on 1 January 2024).

Chilingarian, A., Sargsyan, B., 2024b. Atmospheric positron flux modulation during thunderstorms. Phys. Rev. D 109, 062003. https://doi.org/10.1103/PhysRevD.109.062003.

Chilingarian, A., Sargsyan, B., 2024c. The causes of the abrupt enhancement of the natural gamma radiation in the thunderous atmosphere on the mountain tops. J. Environ. Radioact. 274, 107409 https://doi.org/10.1016/j.jenvrad.2024.107409.

Chilingarian, A., Daryan, A., Arakelyan, K., et al., 2010. Ground-based observations of Thunderstorm-correlated fluxes of high-energy electrons, gamma rays, and neutrons. Phys. Rev. D 82, 043009. https://doi.org/10.1103/PhysRevD.82.043009.

Chilingarian, A., Hovsepyan, G., Hovhannisyan, A., 2011. Particle bursts from thunderclouds: natural particle accelerators above our heads. Phys. Rev. D 83, 062001. https://doi.org/10.1103/PhysRevD.83.062001.

Chilingarian, A., Mailyan, B., Vanyan, L., 2012a. Recovering the energy spectra of electrons and gamma rays coming from the thunderclouds. Atmos. Res. 114–115, 1. https://doi.org/10.1016/j.atmosres.2012.05.008.

Chilingarian, A., Bostanjyan, N., Vanyan, L., 2012b. Neutron bursts associated with thunderstorms. Phys. Rev. D 85 (2012), 085017. https://doi.org/10.1103/PhysRevD.85.085017.

Chilingarian, A., Babayan, V., Karapetyan, T., et al., 2018. The SEVAN Worldwide network of particle detectors: 10 years of operation. Adv. Space Res. 61, 2680–2696. https://doi.org/10.1016/j.asr.2018.02.030.

Chilingarian, A., Mkrtchyan, H., Karapetyan, T., Chilingaryan, S., Sargsyan, B., Arestakesyan, A., 2019. Catalog of 2017 thunderstorm ground enhancement (TGE) events observed on Aragats. Nature Scientific Reports 9 (1), 6253. https://doi.org/10.1038/s41598-019-42786-7.

Chilingarian, A., Hovsepyan, G., Sargsyan, B., 2020. Circulation of Radon progeny in the terrestrial atmosphere during thunderstorms. Geophys. Res. Lett. 47, e2020GL091155 https://doi.org/10.1029/2020GL091155.

Chilingarian, A., Karapetyan, T., Zazyan, M., Hovsepyan, G., Sargsyan, B., Nikolova, N., Angelov, H., Chum, J., Langer, R., 2021a. Maximum strength of the atmospheric electric field. PRD 103, 043021. https://doi.org/10.1103/PhysRevD.103.043021, 2021.

Chilingarian, G. Hovsepyan, Svechnikova, E., Zazyan, M., 2021b. Electrical structure of the thundercloud and operation of the electron accelerator inside it. Astropart. Phys. 132, 102615 https://doi.org/10.1016/j.astropartphys.2021.102615.

Chilingarian, A., Hovsepyan, G., Zazyan, M., 2021c. Measurement of TGE particle energy spectra: an insight in the cloud charge structure. Europhys. Lett. 134, 6901. https://doi.org/10.1209/0295-5075/ac0dfa.

Chilingarian, A., Hovsepyan, G., Zazyan, M., 2021d. Muon tomography of charged structures in the atmospheric electric field. Geophys. Res. Lett. 48, e2021GL094594 https://doi.org/10.1029/2021GL094594.

Chilingarian, A., Kozliner, L., Sargsyan, B., Soghomonyan, S., Chilingaryan, S., Pokhsraryan, D., Zazyan, M., 2022a. Thunderstorm ground enhancements: multivariate analysis of 12 years of observations. Phys. Rev. D 106, 082004. https://doi.org/10.1103/PhysRevD.106.082004.

Chilingarian, A., Hovsepyan, G., Karapetyan, T., Kozliner, L., Chilingaryan, S., Pokhsraryan, D., Sargsyan, B., 2022c. The horizontal profile of the atmospheric electric fields as measured during thunderstorms by the network of NaI spectrometers located on the slopes of Mt. Aragats. J. Instrum. 17, P10011 https://doi.org/10.1088/1748-0221/17/10/P10011.

Chilingarian, A., Hovsepyan, G., Aslanyan, D., Karapetyan, T., Sargsyan, B., Zazyan, M., 2023. TGE electron energy spectra: Comment on "Radar diagnosis of the thundercloud electron accelerator". In: Williams, E., et al. (Eds.), J. Geophys. Res. Atmos. 128, e2022JD037309 https://doi.org/10.1029/2022JD037309, 2022b.

Chilingarian, A., Karapetyan, T., Sargsyan, B., Knapp, J., Walter, M., Rehm, T., 2024. Energy spectra of the first TGE observed on Zugspitze by the SEVAN light detector compared with the energetic TGE observed on Aragats. Astropart. Phys. 156, 02924 https://doi.org/10.1016/j.astropartphys.2024.102924.

Chum, R. Langer, BaŠe, J., Kollárik, M., Strhárský, I., Diendorfer, G., Rusz, J., 2020. Significant enhancements of secondary cosmic rays and electric field at high mountain peak during thunderstorms. Earth Planets Space 72, 28. https://doi.org/10.1186/s40623-020-01155-9.

1 DAVIS weather station. available online: https://www.davisweatherstation.com/. (Accessed 1 January 2024).

Dwyer, J.R., 2003. A fundamental limit on electric fields in air. Geophys. Res. Lett. 30, 2055. https://doi.org/10.1029/2003GL017781.

Gurevich, A.V., Milikh, G.M., Roussel-Dupre, R.A., 1992. Runaway electron mechanism of air breakdown and preconditioning during a thunderstorm. Phys. Lett. 165A, 463. https://doi.org/10.1016/0375-9601(92)90348-P.

Halliday, E.C., 1934. Thunderstorms and the penetrating radiation. Proc. Cambridge Philos. Soc. 30, 206–215. https://doi.org/10.1017/S0305004100016649.

Halliday, E.C., 1941. The thundercloud as a source of penetrating particles. Phys. Rev. 60, 101–106. https://doi.org/10.1103/PhysRev.60.101.

Heck, D., Knapp, J., Capdevielle, J.N., Schatz, G., Thouw, T., 1998. Forschungszentrum (Nuclear Research Center). Karlsruhe, Report No. FZKA 6019.

Hossain, I., Sharip, N., Viswanathan, K.K., 2012. Efficiency and resolution of HPGe and NaI(Tl) detectors using gamma-ray spectroscopy. Sci. Res. Essays 7 (1), 86. https://doi.org/10.5897/SRE11.1717.

Küttener, J., 1950. The electrical and meteorological conditions inside thunderclouds. J. Meteorol. 7, 322–332. https://doi.org/10.1175/1520-0469(1950)007<0322:TEAMCI>2.0. CO;2.

Marshall, T.C., McCarthy, M.P., Rust, W.D., 1995. Electric field magnitudes and lightning initiation in thunderstorms. J. Geophys. Res. 100, 7097. https://doi.org/10.1029/95JD00020.

Nag, A., Rakov, V., 2009. Some inferences on the role of lower positive charge region. in facilitating different types of lightning. Geophys. Res. Lett. 36, L05815.

Roussel-Dupré, R., Symbalisty, E., Taranenko, Y., Yukhimuk, V., 1998. Simulations of high-altitude discharges initiated by runaway breakdown. J. Atmos. Sol. Terr. Phys. 60, 917–940. https://doi.org/10.1016/S1364-6826(98)00028-5.

Schonland, B.F.J., 1930. Thunder-storms and the penetrating radiation. Proc. R. Soc. London, A 130, 37–63. https://doi.org/10.1098/rspa.1930.0187.

Schonland, B.F.J., Viljoen, J.P.T., 1933. On penetrating radiation from thunderclouds. Proc. R. Soc. London, A 314, 314–333.

Spread. available online: https://www.omnicalculator.com/physics/cloud-base. (Accessed 1 January 2024).

Stolzenburg, M.T., Marshall, T.C., Bruning, W.D.E., MacGorman, D.R., T, T., 2007. Electric ield values observed near lightning flash initiations. Geophys. Res. Lett. 34, L04804 https://doi.org/10.1029/2006GL028777.

Wilson, C.T.R., 1921. Investigations on lightning discharges and the electric field of thunderstorms. Philos. Trans. R. Soc. London A. 221, 73–115. https://doi.org/10.1098/rsta.1921.0003.

Wilson, C.T.R., 1925. The acceleration of betta-particles in strong electric fields such as those of thunder-clouds. Proc. Camb. Philos. Soc. 22 (1924), 534. doi:10.1017/s0305004100003236.